Quantitative Characterization of Obliquely Deposited Substrates of Gold by Atomic Force Microscopy: Influence of Substrate Topography on Anchoring of Liquid Crystals

Justin J. Skaife and Nicholas L. Abbott*

Department of Chemical Engineering, University of Wisconsin, Madison, Wisconsin 53706

Received July 10, 1998. Revised Manuscript Received November 12, 1998

We report the use of atomic force microscopy (AFM) to characterize quantitatively the structural anisotropy within ultrathin (thickness of ∼10 nm) *obliquely* deposited films of gold and thereby calculate the influence of this anisotropy on the orientations of liquid crystals (LCs) supported on these surfaces. Whereas visual inspection of AFM images (real space or reciprocal space) reveals no obvious structural anisotropy within these gold films, a quantitative analysis of the AFM profiles does show a subtle level of anisotropy on wavelengths comparable to the lateral dimensions of the gold grains (∼30 nm). Our analysis reveals the root-mean-square (rms) slope of the surface topography to be ∼1° greater in a direction parallel to the direction of deposition of the gold as compared to the perpendicular direction. We also demonstrate the rms curvature of the grains of gold to be greatest in a direction parallel to deposition. Because the amplitude of the surface roughness (∼2 nm) is small compared to its wavelength (∼30 nm), the influence of the surface roughness on the orientations of supported LCs can be described through an elastic mechanism of anchoring. By combining the multimode Berreman-de Gennes model for the elastic free energy density of a nematic LC with AFM profiles of the topography of obliquely deposited gold films, we calculate the azimuthal anchoring energy of the supported LC to be ∼0.015 mJ/m^2, a value that is consistent with estimates of anchoring energies obtained by fabrication of twisted nematic LC cells. The results reported in this paper provide a route to the characterization of surfaces with *designed* levels of anisotropy suitable for control of the anchoring of LCs. This capability will, we believe, find application in studies aimed at exploring the use of LCs for amplification and transduction of events of molecular recognition (e.g., antigen−antibody) at surfaces.

1. Introduction

We have recently reported the anchoring of liquid crystals (LCs) by self-assembled monolayers (SAMs) formed from ω-functionalized alkanethiols supported on films of gold deposited obliquely onto glass substrates.[1−7] Self-assembled monolayers prepared on obliquely deposited films of gold form a useful experimental system for investigations of LCs because, with relative ease, it is possible to design and synthesize surfaces that differ systematically in structure and thus explore the influence of the structure of surfaces on the orientations of supported LCs.[1−7] For example, by hosting ligands for specific proteins within SAMs, we have demonstrated that it is possible to amplify and optically transduce the binding of proteins to these surfaces through the orientations assumed by LCs placed on these surfaces.[7] This approach makes possible visual detection of the binding of proteins to surfaces (including antibody−antigen interactions).

Whereas past studies of SAMs on metals have focused on the use of single crystals of metals,[8−16] metals deposited by electroless methods,[17−21] or evaporated

* To whom correspondence should be addressed. E-mail: abbott@engr.wisc.edu. Fax: 608-262-5434.

(1) Drawhorn, R. A.; Abbott, N. L. *J. Phys. Chem.* **1995**, *99*, 16511.
(2) Gupta, V. K.; Abbott, N. L. *Science* **1997**, *276*, 1533.
(3) Gupta, V. K.; Abbott, N. L. *Phys. Rev. E* **1996**, *54*, R4540.
(4) Miller, W. J.; Abbott, N. L.; Paul, J. D.; Prentiss, M. *Appl. Phys. Lett.* **1996**, *69*, 1852.
(5) Gupta, V. K.; Miller, W. J.; Pike, C. L.; Abbott, N. L. *Chem. Mater.* **1996**, *8*, 1366.
(6) Gupta, V. K.; Abbott, N. L. *Langmuir* **1996**, *12*, 2587.
(7) Gupta, V. K.; Skaife, J. J.; Dubrovsky, T. B.; Abbott, N. L. *Science* **1998**, *279*, 2077.
(8) Strong, L.; Whitesides, G. M. *Langmuir* **1988**, *4*, 546.
(9) Widrig, C. A.; Alves, C. A.; Porter, M. D. *J. Am. Chem. Soc.* **1991**, *113*, 2805.
(10) Chidsey, C. E. D.; Liu, G.-Y.; Rowntree, P.; Scoles, G. *J. Chem. Phys.* **1989**, *91*, 4421.
(11) Camillone, N., III; Chidsey, C. E. D.; Liu, G.-Y.; Putvinski, T. M.; Scoles G. *J. Chem. Phys.* **1991**, *94*, 8493.
(12) Camillone, N., III; Chidsey, C. E. D.; Liu, G.-Y.; Scoles G. *J. Chem. Phys.* **1993**, *98*, 4234.
(13) Dubois, L. H.; Zegarski, B. R.; Nuzzo, R. G. *J. Chem. Phys.* **1993**, *98*, 678.
(14) Samant, M. G.; Brown, C. A.; Gordon J. G. *Langmuir* **1991**, *7*, 437.
(15) Alves, C. A.; Smith, E. L.; Porter, M. D. *J. Am. Chem. Soc.* **1992**, *114*, 1222.
(16) Nuzzo, R. G.; Korenic, E. M.; Dubois, L. H. *J. Chem. Phys.* **1990**, *93*, *767*.
(17) Hou, Z.; Abbott, N. L.; Stroeve, P. *Langmuir* **1998**, *14*, 3287.
(18) Xia, Y. A.; Venkateswaran, N.; Qin, D.; Tien, J.; Whitesides, G. M. *Langmuir* **1998**, *14*, 363.
(19) Menon, V. P.; Martin, C. R. *J. Anal. Chem.* **1995**, *67*, 1920.

10.1021/cm9804822 CCC: $18.00
Published on Web 02/06/1999

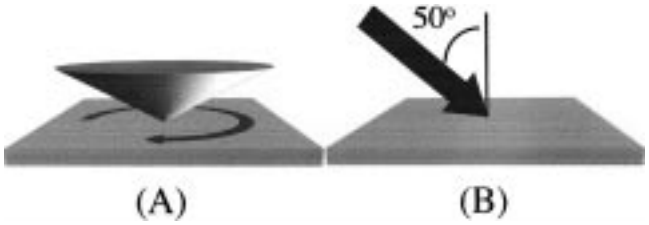

Figure 1. Schematic illustration of procedures used to deposit films of gold. (A) Uniformly deposited films of gold prepared by changing the azimuthal and polar angles of incidence of the gold vapor during deposition. The cone contains the set of all vectors that represent the direction of incidence of the gold vapor. The azimuthal angle of incidence varies from 0° to 360° during evaporation. The polar angle of incidence, measured from the normal of the surface, varies from ~0° to ~70°. (B) Obliquely deposited films of gold. The sample is held stationary during the oblique deposition. The gold is deposited onto the substrate from a unique direction and at an angle of incidence of 50° from the normal of the surface of the substrate. The plane of incidence is defined as the plane that contains the surface normal and the vector representing the incident flux of vapor.

films of metals deposited without a preferred direction (Figure 1A),[1,5] our recent work dealing with the anchoring of LCs on SAMs has relied on the use of gold films deposited at a fixed angle and direction of incidence (Figure 1B).[2−7] We have observed that LCs supported on SAMs formed from alkanethiols on obliquely deposited gold (10 nm of gold deposited at an angle of 50° from the normal) generally assume one of two azimuthal orientations (defined with respect to the plane of incidence of the gold during deposition of the gold film).[3] For example, nematic phases of 4-cyano-4′-pentylbiphenyl (5CB) supported on SAMs formed from $CH_3(CH_2)_{15}SH$ assume an orientation that is parallel to the surface of the substrate and *parallel* to the plane of incidence of the gold during deposition of the film of gold. In contrast, nematic phases of 5CB supported on SAMs formed from $CH_3(CH_2)_{14}SH$ assume an orientation that is parallel to the surface of the gold substrate but *perpendicular* to the plane of incidence of the flux of gold. We also note that attachment of certain nanometer-scale structures to these surfaces (e.g., protein molecules bound specifically to ligands hosted on these surfaces) can *erase* the influence of the obliquely deposited gold on the preferred azimuthal orientations of the supported LC. This fact was exploited in our past work aimed at establishing principles for amplification and transduction of the specific binding of proteins at surfaces.[7]

Although our past studies[2−7] have demonstrated that obliquely deposited films of gold are useful substrates for SAMs when anchoring LCs, the structure of these gold films has not been reported in detail. It is noteworthy that our preliminary attempts to characterize these films by visual inspection of scanning tunneling micrographs did not reveal anisotropy.[6] Although several past studies have reported investigations of the structure of obliquely deposited gold films (using glass substrates), these studies involved the deposition of films of gold under conditions different from those used by us and/or used methods to characterize the gold films that do not provide an obvious connection to the anchoring of LCs.[22−28] For example, by using electron diffraction, Kakati and Wilman have observed that obliquely deposited gold films develop a random crystallographic orientation during the initial stage of growth (<10 nm).[28] This random crystallographic orientation evolves into {111} orientation within thicker films. Films thicker than ~10 nm exhibit a {111} + {111} twin orientation corresponding to a tilt of grains toward the direction of the gold source. We note, however, that films of gold prepared by Kakati and Wilman were deposited at 3 nm/s, whereas our studies of the anchoring of LCs have been performed on films of gold deposited at 0.02 nm/s. Chopra and Randlett reported that obliquely deposited gold films evaporated at slow rates (0.036 nm/s) tend to form contiguous films at smaller thicknesses than films deposited at high rates.[26] Their measurements suggest that deposition rates less than 0.1 nm/s lead to gold films that become contiguous at thicknesses of ~7 nm. These authors also noted that slow deposition rates resulted in the formation of small islands and that columnar growth of grains is only observed after the film is physically contiguous. Kawabata and Ichiji used return path ellipsometry to investigate the optical properties of obliquely deposited gold films comparable in thicknesses to samples used in our experiments and prepared with a deposition rate of 0.02 nm/s.[27] They found that thin films (thickness of ~7 nm) do not show a tilt of the optical axis toward the direction of incidence of the gold while thicker films (~21 nm in thickness) do. These measurements are consistent with results of Kakati and Wilman.[28] Finally, we note that Janning, and Dixon and co-workers have shown that obliquely deposited gold films can be used to preferentially orient LCs.[22,24] The structure of the gold films used to orient the LCs was not, however, investigated.

In this paper, we report an investigation of the structure of obliquely deposited films of gold. The investigation reported in this paper differs from those summarized above in two principal ways. First, we have prepared gold films at low rates of deposition (~0.02 nm/s) using a titanium (Ti) adhesion layer (~1 nm) to promote adhesion between the glass substrates and gold. We have observed the presence of the Ti adhesion layer to influence anchoring of LCs supported on SAMs. We have been unable to observe the "odd−even" effect of alkanethiols (as described above) when using gold films prepared without the titanium adhesion layer. We infer from this result that the structures of thin gold films deposited with and without the Ti adhesion layer are different. Omission of the Ti layer leads to flaking of the gold from the glass substrate. Second, in contrast to past studies, we report experimental procedures and methods of analysis that provide *quantitative* measures of the anisotropy within obliquely deposited gold films such that the anchoring energies of LCs on these

(20) Nishizawa, M.; Menon, V. P.; Martin, C. R. *Science* **1995**, *268*, 700.
(21) Jirage, K. B.; Hulteen, J. C.; Martin, C. R. *Science* **1997**, *278*, 655.
(22) Janning, J. L. *Appl. Phys. Lett.* **1972**, *21*, 172.
(23) Kakati, K. K. *Ind. J. Pure Appl. Phys.* **1977**, *15*, 530.
(24) Dixon, G. D.; Brody, T. P.; Hester W. A. *Appl. Phys. Lett.* **1974**, *24*, 47.
(25) Takeda, S. *Thin Solid Films* **1996**, *281*, 539.
(26) Chopra, K. L.; Randlett, M. R. *J. Appl. Phys.* **1968**, *39*, 1874.
(27) Kawabata, S.; Ichiji, K. *Surf. Sci.* **1976**, *56*, 316.
(28) Kakati, K. K.; Wilman, H. *J. Phys. D: Appl. Phys.* **1980**, *13*, 1477.

substrates can be calculated. We also demonstrate that the measured anisotropy can indeed provide an account of the preferred azimuthal orientation of LCs on obliquely deposited films of gold.

The experiments reported in this paper were performed with the aim of addressing three principal issues related to obliquely deposited films of gold:

First, we aimed to determine if it is possible to detect anisotropy within ultrathin, semitransparent, obliquely deposited films of gold by using AFM or STM. The films of obliquely deposited gold used by us are thin [10 nm, so as to be semitransparent (∼50% transmission)], are formed of small grains with characteristic dimensions of <30 nm, and were reported in a past study to possess no obvious anisotropy when images (real or Fourier space) obtained by AFM or STM were inspected visually.[6] By exercising substantial care in (i) the preparation of substrates onto which gold was deposited, (ii) the preparation of the gold source used to deposit the film, (iii) the use of scanning probe methods (AFM/STM), we report in this paper that it is possible to routinely and reproducibly detect anisotropy within thin, obliquely deposited gold films by using AFM in combination with quantitative methods of image analysis (see below).

Second, we aimed to develop quantitative methods of image analysis that characterize the anisotropy within these films in terms of structural properties of the surface that can be used to predict the orientations of supported LCs. Past studies have demonstrated that the mechanism through which the topography of a surface influences the orientations of supported LCs depends on the wavelength (λ) and amplitude (A) of the roughness of the surface (as well as other factors).[35−41] Only when $\lambda^2/A > L$, where L is the coherence length of the LC, is it possible to described the influence of the roughness of the surface in terms of the elastic deformation of the LC (using bulk elastic constants).[42] For example, short-wavelength, large-amplitude roughness (for which $\lambda^2/A < L$) can cause a decrease in the orientational order within the LC in the near surface region and thus change the local elastic constants of the LC. In this paper, we characterize the anisotropic topography of the gold films by measuring the contour length of cross sectional profiles, the mean curvature of the profiles, and the power spectrum of the cross sectional profiles, all obtained by using AFM. We establish that the criterion $\lambda^2/A > L$ is satisfied on these surfaces and thus describes the anchoring of LCs on these surfaces in terms of an elastic free energy stored within the LCs.

Third, we aimed to determine if the elastic anchoring energy calculated from the structure of the surface (as describe above) can provide an account of the measured strength of azimuthal anchoring of LCs on gold films deposited obliquely. This step is important in order to determine if the anisotropy quantified by AFM is, in fact, responsible for the alignment of LCs supported on these surfaces. In this paper we report that the free energy density of the LC calculated from the nanometer-scale profile of the surface (obtained by AFM) is consistent with an estimate of the anchoring energy obtained by preparing twisted nematic LC cells. We conclude that minimization of elastic deformation of the LC near the surface is an important factor in determining the orientations of LCs on these surfaces. As detailed in the Discussion, this situation differs substantially from obliquely deposited SiO_x and rubbed polymer films, where the elastic mechanism of anchoring is not believed to be the dominant one.

The results reported in this paper—namely, characterization of structural anisotropy within obliquely deposited films of gold—provide a first step toward understanding a variety of LC phenomena on these surfaces, including the manner in which the formation of SAMs and binding of proteins on these surfaces change the orientations of supported LCs (e.g., the dependence of the azimuthal orientation of LCs on the structure of SAMs). These results provide a pathway to the design of gold surfaces that differ systematically in their anisotropy. The capability to control the level of structural anisotropy within these gold films should make possible, for example, the design of surfaces that permit detection of the binding of proteins (or other analytes) at differing threshold concentrations of analyte.

2. Materials and Experimental Methods

Materials. Titanium (99.999%) and gold (99.999%) were obtained from International Advanced Materials (New York, NY). The glass microscope slides were Fisher's Finest, Premium Grade obtained from Fisher Scientific (Pittsburgh, PA). Propanethiol (99%) was obtained from Aldrich (Milwaukee, WI). All aqueous solutions were prepared with Milli-Q water (18 MΩ cm). Acids (H_2SO_4, HNO_3, HCl), bases (KOH), and oxidizer (H_2O_2) were obtained from Fisher. The nematic liquid crystal 5CB was obtained from EM Sciences (New York, NY).

Methods. At the outset of this investigation, we encountered substantial difficulty preparing films of gold that consistently displayed (by AFM) the anisotropy described in the sections below. The procedures reported below were adopted in response to our initial difficulties. We found it necessary to take particular care when (i) cleaning the glass substrates and (ii) cleaning the gold and titanium sources used for the electron beam deposition of the metals. After adopting these procedures, we found it was possible to prepare and characterize the gold films with a high level of reproducibility (see statements below).

2.1. Preparation of Glass Substrates. We characterized the surfaces of a variety of glass microscope slides by AFM (see section 2.3) and frequently found the surfaces of the slides

(29) Jerome, B. *Rep. Prog. Phys.* **1991**, *54*, 391.
(30) Tait, R. N.; Smy, T.; Brett, M. J. *J. Vac. Technol. A* **1992**, *10*, 1518.
(31) van Kranenburg, H.; Lodder, C. *Mater. Sci., Engr.* **1994**, *R11*, 295.
(32) Varnier, F.; Llebaria, A.; Rasigni, G. *J. Vac. Sci. Technol. A* **1991**, *9*, 563.
(33) Mbise, G.; Smith, G. B.; Granqvist, C. G. *Thin Solid Films* **1989**, *174*, L123.
(34) Goodman, L. A.; McGinn, J. T.; Anderson, C. H.; Digeronimo, F. *IEEE Trans. Elec. Dev.* **1977**, *ED-24*, 795.
(35) Wolff, U.; Greubel, W.; Kruger, H. *Mol. Cryst., Liq. Cryst.* **1973**, *23*, 187.
(36) Berreman, D. W. *Phy. Rev. Lett.* **1972**, *28*, 1683.
(37) Barberi, R.; Giocondo, M.; Sayko, G. V.; Zvezdin, A. K. *Phys. Lett. A* **1996**, *213*, 293.
(38) Berreman, D. W. *Mol. Cryst., Liq. Cryst.* **1973**, *23*, 215.
(39) Barberi, R.; Giocondo, M.; Sayko, G. V.; Zvezdin, A. K. *J. Phys.: Condens. Matt.* **1994**, *6*, A275.
(40) Blinov, L. M.; Durand, G.; Yablonsky, S. V. *J. Phys. II Fr.* **1992**, *2*, 1287.
(41) Bodammer, G.; Gourlay, J.; Vass, D. G.; Hossack, W. J. *SPIE* **1995**, *2731*, 95.
(42) De Gennes, P. G.; Prost, J. *The Physics of Liquid Crystals*; Oxford University Press: Oxford, 1993.

to be covered by a soft film (a few nanometers in thickness), parts of which could be easily displaced by imaging the surface in "contact mode". To minimize the extent of formation of this layer on the surface, we stored all glass slides in a dry vacuum desiccator.[43] We found that cleaning procedures based on "piranha solution" alone were not effective in removing this film from the surface of the glass slide. Therefore, we used the following cleaning procedure.

The glass slides were (a) immersed in a piranha [70:30 (% v/v) H_2SO_4:H_2O_2 (30%)] bath at 60−80 °C for at least 1 h (**Warning: piranha solution reacts strongly with organic compounds and should be handled with extreme caution; do not store the solution in closed containers.)**, nitrogen gas being sparged through the solution to provide agitation; (b) rinsed in running 18 MΩ cm H_2O for at least 2 min; (c) immersed in a base [80:20 (% v/v) KOH 2M:H_2O_2 (30%)] solution (with N_2 agitation) and heated to between 60 and 80 °C for at least 1 h; (d) rinsed under 18 MΩ cm water for 2 min; (e) drained of water and then rinsed with ethanol several times without permitting the surface of the slide to dry; (f) drained of ethanol and then rinsed three times using methanol; (g) drained of methanol and then immediately dried under a stream of N_2 for no less than 2 min; (h) placed in an oven at 90 °C for a minimum of 12 h (but typically not longer than 72 h); (i) placed in a vacuum oven and baked under vacuum for a minimum of 2 h at 150−200 °C, the oven being purged with dry N_2 during the cooling cycle; and (j) cooled (in the vacuum oven with a positive N_2 flow) and then immediately placed in the vacuum chamber of the evaporator. The chamber was rapidly pumped down to <0.1 Torr and then purged with N_2 to approximately ∼700 Torr to facilitate the removal of water vapor from the chamber. The chamber was then pumped down to a maximum pressure of 3×10^{-6} Torr before depositing the metals.

2.2. Electron-Beam Deposition of Metals. Metal films of titanium (thickness ∼1 nm) and gold (thickness ∼10 nm) were evaporated onto clean glass substrates with an electron beam evaporator (model SEC600, CHA Industries, Fremont, CA) in a class 100 cleanroom. Prior to placing the gold source in the chamber, the source was visually inspected for unusual surface characteristics (shine, crystallites, etc.). Before deposition, both metal sources were preheated in the chamber (with the deposition shutter closed) to uniformly melt the surface of the metal and thereby expel surface contaminants. Visual inspection during preheating and deposition was used to determine whether the gold source needed to be cleaned. A "slag" of small particles was generally observed to form on the surface of the melt after 10−30 depositions. When a slag was observed, the source was cleaned by immersion (minimum of three cycles, each of 15 min) in aqua regia [20:80 (% v/v) HCl:HNO_3] and piranha solution (see above) at 90 °C. The Au source was cycled between baths until its "brilliant" appearance was restored. After each evaporation, the titanium and gold sources were removed from the chamber.

Prior to depositing a metal film, the chamber was visually inspected, vacuumed, and wiped clean with a solvent-free cleanroom cloth. During each deposition, all parameters indicative of the state of the evaporator were noted (pressures, appearances of metals, and rate of deposition). Typical initial pressures were $<3 \times 10^{-6}$ Torr. During deposition of the gold, the pressure was observed not to rise above 4×10^{-6} Torr. The rate of deposition was controlled by a quartz crystal microbalance (QCM) feedback controller at 0.02 nm/s. The maximum deviation in the rate of deposition was observed at the start of the deposition (for ∼3 s): the rate was always <0.04 nm/s. During deposition of the gold, variations in the rate of deposition of the metal were not measurable (<0.01 nm/s). The thickness of the film was calculated from the value deposited on the QCM and adjusted for the oblique angle of deposition and the position of the slides in the vacuum chamber of the evaporator.

Obliquely deposited films of gold were prepared by holding the glass substrates stationary during deposition of the gold (Figure 1B). The incident vapor was deposited at an angle of 50° measured from the normal of the slide. The preferred direction of deposition of the metal leads to the creation of structural anisotropy within the metal film (see below). A principal cause of anisotropy within obliquely deposited films of metals is believed to be self-shadowing of the incident metal vapor.[31] In contrast, so-called "uniformly deposited films of gold" were prepared by varying both the polar and azimuthal angles of incidence of the gold onto the substrate during the evaporation (Figure 1A). The motion of the slides was controlled by their mounting on a planetary that rotated with an epicyclical motion about the vertical axis of the evaporator. Due to the motion of the substrate, the gold was deposited onto the substrate without a preferred direction (and thus no structural anisotropy formed within the gold film).

Upon removal of the metal films from the evaporator, we performed AFM analyses on at least one sample from each batch of slides. The AFM analysis was used to screen for the presence of defects or debris (>100 nm in size) on the surface of the film. We typically observed no debris or defects within an area with lateral dimensions of 5 μm. Our experience has been that samples showing defects/debris within 5 μm × 5 μm areas will lead to erroneous analyses (as described below). Following each deposition, we also measured the orientations of bulk LCs supported on SAMs formed on the gold films. We confirmed our past results[1,7] by using a polarized light microscope (BX60, Olympus) with a quarter wave plate. Samples of gold that did not pass the two tests described above were not further investigated. With the cleaning and deposition procedures reported above, however, we found that almost all depositions were successful (>90%).

2.3. Atomic Force Microscopy. We used AFM to characterize the nanometer-scale structure of the gold films. We used AFM rather than STM (although we have also performed STM with results similar to those reported in this paper using AFM) because a goal of our future work is to characterize obliquely deposited films of gold supporting SAMs formed from alkanethiols (e.g., hexadecanethiol) as well as proteins bound specifically to ligands on these surfaces. These future studies will require the use of AFM and not STM.

The AFM used in this study was a Nanoscope III (Digital Instruments, Santa Barbara, CA). Oxide sharpened silicon nitride tips were used to minimize tip convolution effects. The nominal radius of curvature of the tip was specified by Digital Instruments as 5−40 nm. All samples were scanned under ambient conditions using the "contact mode" and an "E" scanning head (∼15 μm maximum scan size). To obtain AFM images of sufficient quality and reproducibility for use in quantitative analyses of the gold films, we found it necessary to adopt the following procedures.

(a) Sample Preparation. Bare gold samples were imaged within 6 h of deposition and were stored in either a desiccator or a vacuum desiccator. Each sample was immediately moved to the AFM after removal from the desiccator. The samples were glued to steel disks in order to minimize drift that we sometimes observed when gold films were mounted on steel disks using double-sided tape. Each sample was aligned on the scanning piezo using either the parallel or the perpendicular wall of the laser head as a reference with which to align an edge of the sample. No other method of aligning samples was found to be practical due to the confined space within the head of the AFM.

(b) Imaging. The base unit of the AFM was left "on" in order to maintain the unit at a constant temperature. The piezos and laser head were stored in a dry environment and allowed to "warm" for at least 1 h before samples were placed on the piezo. The surface was engaged by the AFM controller with a photodetector setpoint bias of 1.5 V to provide a midrange force during contact. The exact value of the force did not appear to be important. The integral and proportional gains were typically set at 3 and 9, respectively: the gains were sufficiently high to record visually crisp images but low enough to avoid the presence of oscillations in the images. The presence of oscillations was easily checked by observing cross-section plots in real-time. The size of the initial scan was 5

(43) Eskilsson, K.; Yaminsky, V. V. *Langmuir* **1998,** *14,* 2444.

μm. If debris was visible in any of several scans of the surface, the sample was discarded. Since adopting the procedures described above for the preparation of the samples, we have discarded less than 10% of the samples. Following the survey scan, the size of the scan was reduced to 1 μm. During this scan, the condition of the AFM tip was assessed. Any tips producing artifacts (e.g., double images, caused by twin tips, or strikingly similar shapes caused by tip convolution) were removed and discarded. The size of the scan was then reduced to 350 nm: if the resulting scans were not "crisp", the tip was discarded. Otherwise, the images were captured. Less than 20% of the tips tried were found acceptable for use. After capturing several images, the tip was disengaged. The sample was then physically rotated by 90°, and the process described above was repeated (using the same tip). The samples were physically rotated to test for apparent anisotropy within the images that might be caused by the direction of rastering of the tip across the surface.

All images were flattened by using the AFM software which corrects for any large-scale tilt of the sample with respect to the AFM. *No other filtering of the images was performed.* Images analyzed before flattening were found to show the same level of anisotropy as nonflattened images. Flattening does, however, improve the visual appearance of the images. All Fourier analyses were performed on raw (nonflattened) images. Furthermore, we used raw data obtained in the direction of scanning (*x*-axis) to calculate the Fourier spectrum of the surface and thus estimate the elastic energy density of a supported LC. This approach required that the sample be physically rotated by 90° to obtain the one-dimensional Fourier spectra in orthogonal directions on the surface. The AFM was found to produce artificial high-frequency noise in the direction orthogonal to the fast scanning direction of the tip, and all profiles obtained in this direction were found to exhibit large power spectrum amplitudes at large wavevectors. Power spectra obtained from the profiles measured in the *x*-direction were found to be reproducible.

2.4. Anchoring of Liquid Crystals. We measured the orientations of LCs on SAMs formed from $CH_3(CH_2)_2SH$. The SAMs were used to protect the surface from contaminants before injection of the LC. Self-assembled monolayers were formed on the surfaces of the gold films (~10 mm × ~25 mm) by immersion of the films in ethanolic solutions containing 1 mM propanethiol (for 2 h). Substrates were then thoroughly rinsed with ethanol and dried by blowing a stream of N_2 across the surface of the slide. Each piece of gold film was then cut in half (~10 mm × ~12 mm) and placed again under a stream of N_2 to displace any glass shards from the surface. Thin plastic spacers (thickness ~10 μm, Mylar or Saran wrap) were then placed along the edges of an upward-facing half of the gold film. The second half of the sample was then placed, face-down, onto the spacers with an orientation such that the direction of deposition of the gold onto the second sample was orthogonal to the first gold film (as described below, this procedure leads to the formation of a twisted LC within the cell). The cell was held together by using "bulldog" clips placed along the edge of the sample. Both the optical cell and 5CB were then heated to ~40 °C by using a hot plate and air gun. At this temperature, 5CB is an isotropic liquid that readily fills the optical cell by capillarity. Once filled with 5CB, the optical cell was removed from the hot plate and allowed to cool at ~15 °C/min to room temperature.

The optical texture of the cell filled with LC was viewed under a polarized light microscope (in transmission mode). First, the direction of deposition of the gold on one of the surfaces of the optical cell was aligned with either the polarizer or analyzer of the microscope. The presence of ~90° twist deformation within the LC was inferred from the extinction of light with parallel polars and transmission of light with crossed polars. In contrast, the absence of twist was deduced by (I) transmission of light through parallel polars and extinction of light through crossed polars and (II) strong modulation in the intensity of transmitted light (from light to dark) when the sample was rotated between crossed polars.

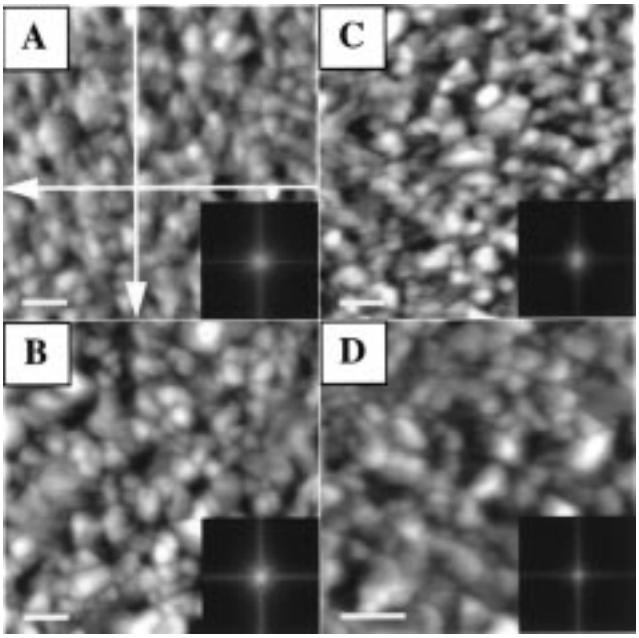

Figure 2. Images of gold films (10 nm of Au on ~1 nm of Ti) obtained by AFM. The insets are fast Fourier transforms of the real-space images. The gray scale of contrast in the real-space images corresponds to a variation in height (*z*-axis) of 8 nm. The horizontal scale bar in each image represents a lateral dimension of 50 nm. The scanning direction (see text for definition) is horizontal in each. (A) 350 nm × 350 nm image of an obliquely deposited film of gold with the direction of deposition parallel to the scanning direction. (B) 350 nm × 350 nm scan of a film of gold deposited uniformly. (C) 350 nm × 350 nm image of an obliquely deposited film of gold with the direction of deposition perpendicular to the scan direction. (D) 250 nm × 250 nm image of an obliquely deposited film of gold with the direction of deposition parallel to the scan direction.

3. Results

3.1. Visual Inspection of Real Space and Fourier Images. Figure 2 shows real-space AFM images of obliquely deposited and uniformly deposited films of gold having thicknesses of 10 nm. In all these images, the horizontal axis corresponds to the "scanning direction" of the AFM, that is, the fast axis (also noted as the *x*-axis) of the AFM head when imaging.

Figure 2A is an image of an obliquely deposited film of gold with lateral dimensions of 350 nm × 350 nm. The scanning direction is parallel to the direction of deposition of the gold in Figure 2A. Inspection of this image shows the surface of the gold film to be "pebbly" in nature, with grains ranging in size from approximately 10 nm to 40 nm. The pebbly nature of the surface can be easily visualized in the three-dimensional plots shown in Figure 3. Figure 3A has a magnified scale in the *z*-direction (by a factor of ~4 relative to lateral dimension). The expanded *z*-scale provides a clearer (although exaggerated) view of the pebble-like texture of the film. Figure 3B, in contrast, shows the three-dimensional plot with lateral and vertical scales that are approximately equal (the vertical scale bar is 64 nm). From Figure 3B, it is apparent that these films are relatively flat (see below for a quantitative statement) with heights ranging approximately ± 2 nm over most of the image.

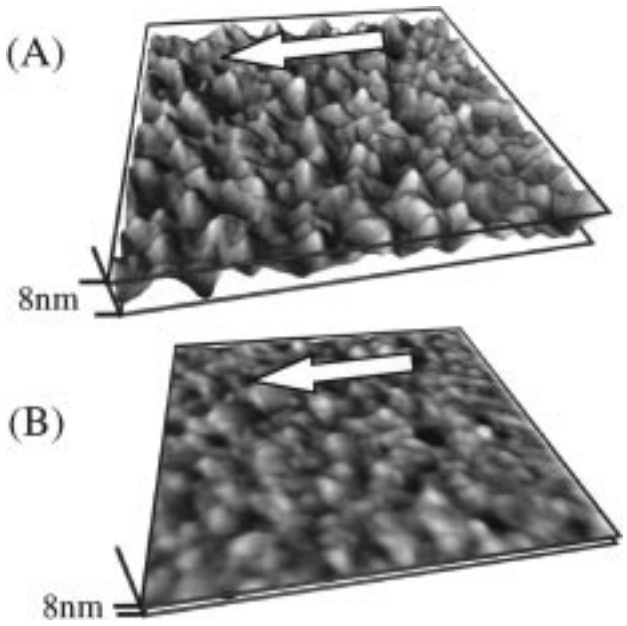

Figure 3. Three-dimensional plots of the AFM image of the obliquely deposited gold film shown in Figure 2A. The white arrow indicates the direction of deposition of the gold film. (A) The vertical scale bar corresponds to a height of 16 nm (expanded *z*-scale). (B) The vertical scale bar corresponds to a height of 64 nm (*z*-scale approximately equal to horizontal scale).

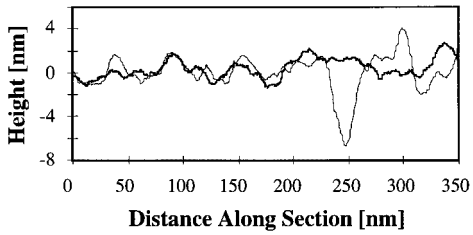

Figure 4. Cross sectional profiles taken from the AFM image of the obliquely deposited film of gold shown in Figure 2A. The white lines in Figure 2A indicate the location of the cross sectional profiles. The thin line represents the cross sectional profile measured parallel to the direction of deposition of the gold film. The thick line represents the cross sectional profiles measured perpendicular to the direction of deposition of the gold film.

Inspection of the images in Figures 2A and 3 shows these gold films to be largely continuous, with the exception of a few holes (dark spots) found in each square micrometer of the surface: these holes have depths comparable to the thickness of the gold film (∼10 nm) (see Figure 4). By using X-ray photoelectron spectroscopy, we detected no evidence of Ti (or of oxides of Ti or Si) at the surface of these evaporated films of gold. Other dark regions observed in the AFM images were only about ∼4 nm deep. These shallow pits are seen in all images (A−D) in Figure 2.

Figure 4 compares cross sectional profiles obtained in orthogonal directions from Figure 2A (indicated by horizontal and vertical lines in Figure 2A). These cross sectional profiles are representative of many that we viewed: no obvious or reproducible differences in roughness can be seen to exist between the cross sections measured in directions parallel and perpendicular to the directions of deposition, except for high-frequency noise that is always present in the slow scanning direction. Similarly, visual inspection of the images and profiles in Figures 2A, 3, and 4 does not reveal any obvious structural anisotropy within these obliquely deposited films of gold. Also, visual inspection of Fourier space images (wavelengths ranging from the sample scan size to approximately 1 nm) reveals no anisotropy within these films. Although we believe we may, in fact, sometimes be able to see anisotropy by visual inspection (e.g., slight elongation of grains perpendicular to deposition direction in Figure 2A), the level of anisotropy is slight and such conclusions vary from one observer (and one sample) to the next. In contrast, the quantitative methods of image analysis described below do consistently reveal the presence of an anisotropic roughness within these films.

Figure 2B shows an image of a gold film (10 nm in thickness) that was deposited without a preferred direction (a so-called "uniformly deposited gold film"). Visual comparison of the films of gold shown in Figure 2A,B shows only subtle differences. The apparent sizes of the gold grains in Figure 2B are slightly larger than those shown in Figure 2A. Only by quantitative analysis can anisotropy be detected in Figure 2A and not Figure 2B.

Because the rastering motion of an AFM tip can introduce artifacts into images (e.g., due to finite response times of the feedback controller and different piezo sensitivities of the *x*- and *y*-directions), we also imaged the obliquely deposited gold film shown in Figure 2A with the scanning direction of the AFM head *perpendicular* to the direction of deposition of the gold. This image is shown in Figure 2C and was obtained by physically rotating the sample under the AFM head (see methods section). We did not use the piezos to change the direction of scanning of the AFM tip across the gold films because a change in the direction of scanning using the piezos can change the level of high-frequency noise caused by the feedback control of the AFM and thus create apparent anisotropy in the images. Following rotation of the sample, the slight elongation of gold grains in the vertical direction of Figure 2A (perpendicular to the direction of deposition of the gold) appears to move to the horizontal direction of the image shown in Figure 2C. This result suggests that the apparent discernible elongation of grains was not due to drift of the sample during rastering of the AFM head. Past studies of obliquely deposited metals (silver and chrome) have reported elongated grains to form in a direction that is perpendicular to the plane of deposition of the metal.[24,44]

Figure 2D is a 250 nm × 250 nm image of an obliquely deposited film of gold, oriented during imaging with the direction of deposition of the gold parallel to the scan direction. This image shows the same qualitative features seen at lower resolution (Figure 2A). Figure 2D is analyzed quantitatively below.

3.2. Contour Analysis. As described above, visual inspection of AFM images shown in Figures 2−4 does not reveal obvious differences between the structures of obliquely and uniformly deposited films of gold nor does it reveal clear differences between the structures of obliquely deposited gold films characterized in directions parallel and perpendicular to the direction of

(44) Smith, D. L. *Thin-Film Deposition: Principles & Practice*; McGraw-Hill: New York, 1995.

deposition. Here we report quantitative analyses of the topography of these films in order to unambiguously identify the existence of structural anisotropy within obliquely deposited films of gold. The first of these analyses is based on the contour length of cross sectional profiles of gold films.

We choose this method of analysis for three reasons. First, it is simple to perform. Second, measurements of contour lengths at different wavelengths and azimuthal orientations (measured with respect to the direction of deposition of the gold) make possible identification of the characteristic spatial scales on which anisotropy exists within the films of gold. Third, because the contour length is related to the average of the square of the local slope of a surface (see below), it forms an intuitively useful index of the structure of a surface. Measurements of contour lengths have been used in the past to obtain the fractal dimensions of metal oxide films.[25,37,39]

We used the following procedure to determine contour lengths from AFM images of thin films of gold. First, AFM images were exported as 512 × 512 matrices. Each element of the matrix represented the height (z_i) of a point on the gold surface. Each matrix was read into a FORTRAN program that calculated the square of the distance between points with heights z_i and $z_{i+\lambda}$ separated by a horizontal distance λ in a known azimuthal direction:

$$\mathrm{cont}^2_{i,\lambda} = \frac{(z_{i+\lambda} - z_i)^2 + \lambda^2}{\lambda^2} \tag{1}$$

From the above equation, the relationship between the local slope of the surface $[(z_i - z_{i+\lambda})/\lambda]$ and contour length is apparent. The average of the square of the contour length was calculated for a family of cross sectional profiles obtained from an AFM image as

$$\overline{\mathrm{cont}^2_{\lambda}} = \sum_i^n \frac{\mathrm{cont}^2_{i,\lambda}}{n} \tag{2}$$

The square root of eq 2 is the root mean square (rms) contour length of the surface. This quantity was calculated from each image for different wavelengths (λ) and azimuthal sampling orientations. When sampling azimuthal orientations not at 0° or 90° (measured from a vector parallel to the direction of scanning), a simple linear interpolation was used to determine the height of sampling points that fell between actual data points in the AFM image. The use of the linear interpolation did not introduce a significant error into our analysis because the minimum wavelength of sampling always covered several experimental data points. Note that the contour length is dimensionless since the measurement is the topological distance traversed while moving a lateral distance of 1 nm.

Before describing the results, we emphasize that a number of precautions were necessary in order to reach reliable conclusions based on a contour analysis. First, we ensured that the minimum wavelength used in the analysis (∼4 nm) corresponded to a minimum spacing of ∼6 pixels for a 350 nm × 350 nm image with 512 × 512 data points. This minimized the introduction of artificial roughness seen at <3 pixel spacing due to inherent feedback oscillations of the AFM. Second, we excluded from the analysis any pixels near the edges of the image (within ∼10 pixels of the edge of the image), since the primary noise due to feedback and the reversal of the tip direction occurs at the edges of a scan. Third, we observed that the rastering of the AFM tip introduces an artificial contribution to the roughness of the surface at orientations perpendicular to the scan direction. Therefore, we physically rotated the sample to determine if the noise was affecting the contour length calculations. If noticeable differences were seen in the contour analyses between the initial sample orientation and the physically rotated orientation, then the data was discarded. Fourth, we found it necessary to operate the AFM with feedback settings that were sufficiently low to reduce oscillations in the image (visually seen near the edges of the scan) but high enough to accurately represent the surface, as previously noted in the AFM methods section.

Figure 5 shows the results of a contour length analysis of the real-space images shown in Figure 2. The *y*-axis represents the dimensionless contour length, and the *x*-axis corresponds to the azimuthal orientation of the contour measured with respect to the direction of scanning (horizontal axis of images in Figure 2). In each panel of Figure 5, contour lengths are reported for values of λ of 4, 8, 12, 20, and 40 nm. In addition, the ordinate axis on the right-hand side of the plots in Figure 5 shows the average (rms) slope of the surface (reported as an angle of inclination measured from the horizontal).

Figures 5A shows the contour lengths and rms slope of the obliquely deposited films of gold shown in Figure 2A; this film was imaged with the deposition direction parallel to the scanning direction. The contour analysis does show anisotropy within this film: the contour length parallel to the direction of deposition of the gold (0°−10°) is greater than the contour length perpendicular to it (90°−100°). The ∼10° displacement of the minimum from 90° is likely caused by uncertainly in the orientation of the sample within the AFM. These results indicate that the rms slope of the gold film (see right axis in Figure 5) is greater when measured parallel to the direction of deposition of the gold (by ∼1°). These results also demonstrate that the anisotropy decays with increasing wavelength of sampling (λ). Anisotropy was not measured when the wavelength was greater than ∼20 nm (see below). The loss of anisotropy at wavelengths >20 nm indicates that the anisotropic structure within the surface exists at spatial scales comparable to or smaller than the sizes of the grains of gold within the film; this conclusion suggests the presence of elongated grains of gold with long axes oriented perpendicular to the direction of deposition of the gold.

Figure 5B shows a contour analysis of an obliquely deposited gold film shown in Figure 2C. Because this sample was imaged with the scan direction perpendicular to the direction of deposition of the gold, if scan artifacts are absent in our analysis, the contour analysis should yield results identical to Figure 5A but shifted

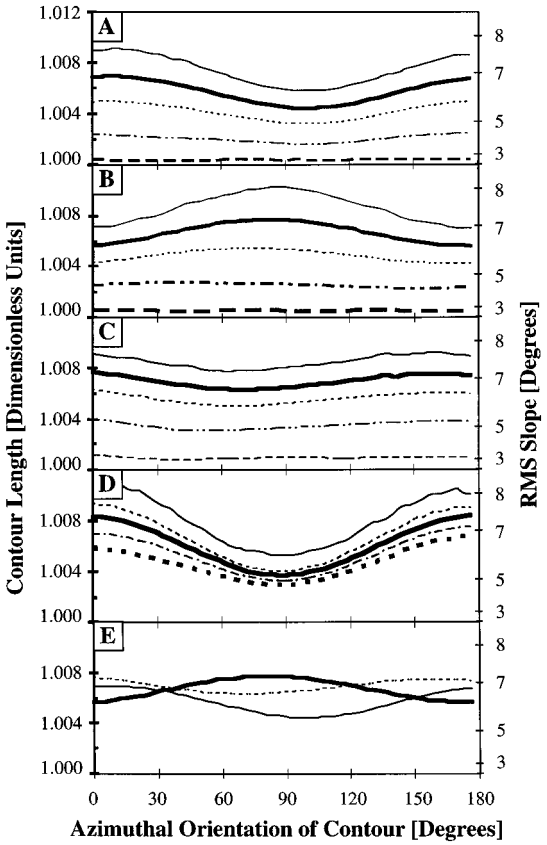

Figure 5. Contour lengths calculated from AFM images of obliquely deposited films of gold shown in Figure 2. Sampling wavelengths in A−C are (−) 4 nm, (—) 8 nm, (···) 12, (-·-) 20, and (- - -) 40 nm. (A) Contour analysis of the obliquely deposited film shown in Figure 2A. An azimuthal orientation of 0° (*x*-axis) corresponds to a contour oriented parallel to the direction of deposition of the gold film. (B) Analysis of the obliquely deposited film shown in Figure 2C. An azimuthal orientation of 0° corresponds to a contour oriented perpendicular to the direction of deposition of the gold film. (C) Analysis of the uniformly deposited film of gold shown in Figure 2B. An azimuthal orientation of 0° corresponds to a contour oriented parallel to the scan direction. (D) Analysis of the obliquely deposited film of gold shown in Figure 2D. An azimuthal orientation of 0° represents a direction that is parallel to the direction of deposition. Sampling wavelengths from top: (−) 2 nm, (- - -) 4 nm, (—) 6, (-·-) 8, and (- - -) 10 nm. (E) Comparison of contour lengths measured using a sampling wavelength of 8 nm: (−) from A, (—) from B, (- - -) from C.

in phase by 90°. This shift is indeed observed. The measured contour length is greatest in a direction parallel to the direction of deposition of the gold and the anisotropy is observed to decay with increasing wavelength. We note, however, that the magnitude of the anisotropy is slightly less in Figure 5A as compared to Figure 5B. This difference is likely caused by local variations in the magnitude of the anisotropy as a function of position on the surface. Note that the experimental procedure used to collect the images in Figure 5A,B requires the rotation of the sample by 90°. The two images shown are not, therefore, from the same location on the surface of the gold film. As described below, these local variations in anisotropy may reflect the roughness of the underlying glass substrates.

Figure 5C shows a family of contour lengths obtained using the uniformly deposited film of gold shown in Figure 2B. In comparison to the obliquely deposited film, the uniform film shows little anisotropy. The azimuthal locations of the minima and maxima were found to vary when uniformly deposited gold films were characterized at several locations on the same sample. We have considered the possibility that the roughness of the glass substrates gives rise to local variations in the angle of incidence of gold during deposition of the film. By using a surface profiler, we measured the roughness of the glass to have an amplitude of ∼10 nm on a wavelength of micrometers. This roughness would give rise to variations in the local angle of incidence of the gold of ∼1°. Whether or not this small variation in the angle of incidence could give rise to the local anisotropy in the gold is unknown. The average contour lengths of the uniformly deposited gold films were typically found to lie between the maximum and minimum contour lengths of the obliquely deposited films.

When using the images in Figure 2A−C, we found that it was not possible to measure the contour lengths using sampling wavelengths smaller than 4 nm because pixelation within these images introduced noise into the contour analysis. Higher resolution images were found to be necessary in order to evaluate contour lengths at shorter wavelengths. Figure 2D is a 250 nm × 250 nm image of an obliquely deposited film. The corresponding contour plot is shown in Figure 5D with wavelengths of 2, 4, 6, 8, and 10 nm. The plot clearly shows that anisotropy is still present at high resolutions and short (2 nm) wavelengths.

To permit a direct comparison of uniformly deposited and obliquely deposited films, Figure 6E shows contour lengths of both types of films for wavelengths of 8 nm. The uniform sample exhibits a contour length that is approximately the average of the orientation-dependent contour lengths of the obliquely deposited films.

In summary, the results above unambiguously establish the presence of structural anisotropy within ultrathin obliquely deposited films of gold. The structural anisotropy is measured over distances on the surface corresponding to the grain size of the gold or smaller; the mean slope of the surface is greatest in a direction parallel to the direction of deposition of gold (by ∼1°).

3.3. Analysis of the Root Mean Square Curvature of the Gold Surface. Whereas the analysis of contour lengths presented above permits identification of anisotropy within the surface in terms of the average slope of the surface (first spatial derivative), LCs on surfaces are influenced by the *curvature of surfaces* (second spatial derivative) and not the local slope. Indeed, it is possible to construct hypothetical surface profiles such that the rms slope differs in orthogonal azimuthal directions yet the curvature is the same.[46] The curvature of a surface can be directly tied

(45) Pidduck, J.; Bryan-Brown, G. P.; Haslam, S.; Bannister, R.; Kitely, I.; McMaster, T. J.; Boogaard, L. *J. Vac. Sci. Technol. A* **1996**, *14*, 1723.

(46) By using two sine functions, it is possible to create a model surface that has equal curvatures but different contour lengths in two orthogonal directions. If one direction is composed of a sinewave with an amplitude A_0 and a wavevector q_0, the corresponding contour length and curvature are proportional to A_0q_0 and $A_0q_0^2$, respectively. If we choose to keep the curvature constant, then the orthogonal sine curve can be described by any new values of A and q that satisfy $A_{new}q_{new}^2 = A_0q_0^2$. All new values of A and q will lead to contour lengths in the orthogonal direction that are different from the original values.

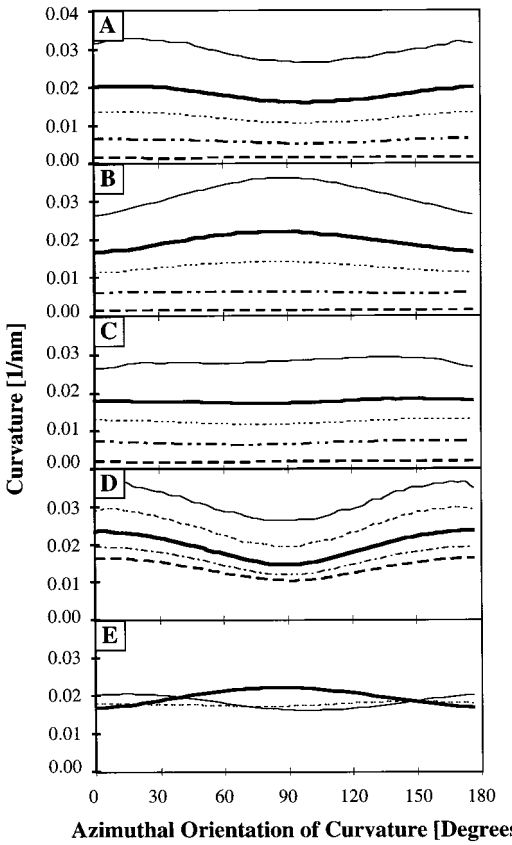

Figure 6. Curvature measured from AFM images of obliquely deposited films of gold shown in Figure 2. Sampling wavelengths in A−C are (−) 4 nm, (—) 8 nm, (···) 12, (-·-) 20, and (- - -) 40 nm. (A) Analysis of the obliquely deposited film shown in Figure 2A. An azimuthal orientation of 0° (*x*-axis) corresponds to a contour oriented parallel to the direction of deposition of the gold film. (B) Analysis of the obliquely deposited film shown in Figure 2C. An azimuthal orientation of 0° corresponds to a contour oriented perpendicular to the direction of deposition of the gold film. (C) Analysis of the uniformly deposited film of gold shown in Figure 2B. An azimuthal orientation of 0° corresponds to a contour oriented parallel to the scan direction. (D) Analysis of the obliquely deposited film of gold shown in Figure 2D. An azimuthal orientation of 0° represents a direction that is parallel to the direction of deposition. Sampling wavelengths from (−) 2 nm, (- - -) 4 nm, (—) 6, (-·-) 8, and (- - -) 10 nm. (E) Comparison of contour lengths measured using a sampling wavelength of 8 nm (−) from A, (—) from B; (- - -) from C.

to the elastic energy density (due to twist, splay, and bend) of a LC placed on the surface by[42]

$$F_d = \frac{1}{2}K_1(\text{div } n)^2 + \frac{1}{2}K_2(n \times \text{curl } n)^2 + \frac{1}{2}K_3(n \times \text{curl } n)^2 \quad (3)$$

where K_1, K_2, and K_3 are the splay, twist, and bend elastic constants, respectively, and n is the director of the LC. Each term in eq 3 possesses a leading order term that is proportional to the curvature of a surface. Below we demonstrate that obliquely deposited gold films do possess anisotropic curvature (i.e., different values of curvature measured in orthogonal directions on the gold surface).

The procedure we used to estimate the curvature of the gold films from AFM images was similar to that reported above for the contour analysis. First, a central point difference method (eq 4) was used to calculate the square of the curvature as a function of wavelength and azimuthal direction at all points on the image (except those near edges):

$$\text{curv}_{i,\lambda}^2 = \left[\frac{z_{i+\lambda} - 2z_i + z_{i-\lambda}}{\lambda^2}\right]^2 \quad (4)$$

The values of the square of the curvature were then averaged for a given azimuthal orientation

$$\overline{\text{cont}_\lambda^2} = \sum_i^n \frac{\text{curv}_{i,\lambda}^2}{n} \quad (5)$$

from which the rms values of curvature were evaluated.

Figure 6 shows the rms curvature of each image shown in Figure 2. The sequence of presentation of plots is the same as that used in Figure 5. In short, the rms curvature of the surface of the obliquely deposited films is greatest in a direction parallel to the direction of deposition of gold on an obliquely deposited gold film (Figure 6A,B,D), whereas the uniformly deposited film of gold does not show evidence of a curvature that changes significantly with azimuthal orientation (Figure 6C). To permit direct comparison of uniformly deposited and obliquely deposited films, Figure 6E shows the curvatures for wavelengths of 8 nm. The uniformly deposited films exhibit rms curvatures that are approximately the average of the orientation-dependent rms curvatures of the obliquely deposited films. It is useful to note that the rms curvatures reported in Figure 6E range from ∼0.018 to ∼0.023 nm^{-1}, which corresponds to radii of curvature between ∼55 and ∼43 nm, respectively. These values are similar in magnitude to the grain size, which indicates that the shapes of the grains likely determine the anisotropic curvature.

The results of the curvature analysis described above confirm the existence of structural anisotropy within the obliquely deposited gold films of a type (curvature) that should influence the orientations of supported LCs. Below, we establish that the magnitude of this curvature is sufficient to account for the azimuthal orientations of LCs supported on obliquely deposited films of gold.

3.6. Estimation of the Anchoring Energy of 5CB from the Topography of Obliquely Deposited Films of Gold. Several past studies have used the Berreman strain model[36,38] to estimate the elastic free energy density of a LC supported on a surface with sinusoidal roughness of one wavelength:

$$F = \frac{K_3}{4}A^2q^3 \quad (6)$$

where A is the amplitude, q is the wavevector of the sine wave, and K_3 is the bend elastic constant of the LC. This model contains a number of approximations, including the assumptions that (i) the director lies across the sinusoidal corrugations, (ii) there exists no (local) azimuthal variations in the orientation of the LC, and (iii) the elastic constants (splay and bend) of the LC are equal. The result above applies to surfaces with

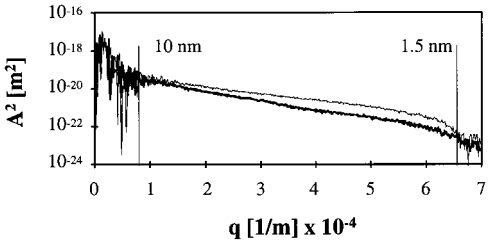

Figure 7. Power spectrum of an obliquely deposited film of gold obtained from the analysis of cross sectional profiles taken from the AFM image in Figure 2C. The thin line is the power spectrum obtained using cross sectional profiles obtained in the direction parallel to the direction of deposition of the gold film. The thick line corresponds to the perpendicular direction. Anisotropy is evident for wavelengths between ~10 and ~1.5 nm.

a single mode of roughness. Obliquely deposited substrates, however, possess a spectrum of wavelengths and amplitudes of roughness.

By using a Fourier representation, an arbitrary surface can be described as a linear superposition of a family of sine waves:

$$z(x) = \sum_k A_k \sin(2\pi x q_k) \tag{7}$$

Although some past studies have evaluated the elastic energy density from such a representation of a surface as

$$F = \frac{K_3}{4}\sum_k A_k^2 q_k^3 \tag{8}$$

we do not believe this method to be generally correct.[37] Although many different sets of $\{A_k, q_k\}$ can be used to represent a given surface profile, the elastic energy density is not the same for each set. This conclusion is supported by the observation that the profile a single mode surface can be described by either a single sine function of amplitude A or by a set of m sine functions with scaled amplitudes A/m; the free energy density given by eq 8 is not the same for both representations of the surface. In contrast, we believe the multimode analysis originally described by Berreman to be correct;[38] this analysis includes the presence of crossed terms in the summation

$$g = \frac{K_3}{2}\sum_j\sum_k A_j A_k\, q_j^2\, q_k^2 \cos[x(q_j - q_k)] \exp[-(q_j - q_k)z] \tag{9}$$

where A_j and A_k are the amplitudes of the Fourier components, q_j and q_k are the associated wavevectors, x is the lateral position along the sine wave, z is the height from the surface, and K_3 is the bend elastic constant. This equation is based on the assumption that all elastic constants of the LC are approximately equal to K_3. Unlike eq 8, any family of sinusoidal functions that accurately represents the profile of the surface will give the same free energy density when using eq 9 (after averaging g over all values of x and integrating from $z = 0$ [the surface] to far from the surface).

Figure 7 shows a plot of A^2 versus q (a so-called power spectrum) for the obliquely deposited film of gold shown in Figure 2A. The amplitudes of each mode of the surface (A shown in Figure 7) in the parallel and perpendicular directions differ appreciably at values of q greater than 1×10^4 m^{-1}, corresponding to wavelengths of ~10 nm, and then converge again at values of q of 7×10^4 m^{-1}, corresponding to wavelengths of ~1.5 nm. The amplitudes of the modes parallel to the direction of deposition of the gold are larger than those in the perpendicular direction. This result is consistent with the contour and curvature analyses described above.

The influence of the roughness of a surface on the elastic energy density of a supported LC can be evaluated using eq 9 only if the constraint $\lambda^2/A > L$ is satisfied. For our experimental system, the surface of a typical gold grain has a lateral dimension of ~20 nm and an amplitude (A) of 2 nm. We calculate, therefore, λ^2/A to be 200 nm. This value is an order of magnitude larger than the typical coherence length of a LC such as 5CB or MBBA (~15 nm).[53] We conclude that the free energy density of a LC supported on an obliquely deposited film of gold (of the type reported in this paper) can be described in terms of an elastic mechanism.

By combining eq 9 with the power spectrum in Figure 7, we have evaluated the difference in the elastic free energy of a LC oriented parallel and perpendicular to the direction of deposition of the gold as

$$\Delta F = |F_{90°} - F_{0°}| \tag{10}$$

For nematic 5CB at room temperature ($K_3 = 10 \times 10^{-9}$ mN),[47] we calculate an anchoring energy of ~0.015 mJ/m^2, with the higher elastic energy corresponding to an orientation of the LC that is parallel to the direction of deposition of the gold. Below, we compare this calculated anchoring energy to that measured using 5CB confined within a twisted cell formed by using obliquely deposited substrates of gold.

3.7. Anchoring of 5CB: An Experimental Bound on the Magnitude of the Azimuthal Anchoring Energy. Within a twisted nematic LC cell (Figure 8A), the interactions of the LC with the confining surfaces must be sufficiently strong to support the formation of the twist deformation within the LC. The twist deformation within the LC can only be formed if the azimuthal anchoring energy exceeds a threshold. By using the azimuthal anchoring energy evaluated above, we estimate the minimum thickness L of a twisted nematic LC cell that can be formed under the influence of an azimuthal anchoring energy ΔF as[42]

$$L = \frac{K_2}{2\Delta F}\left(\frac{\pi}{2}\right)^2 \tag{11}$$

By using a twist elastic constant[47] of 6.4×10^{-9} mN and a value of ΔF of 0.015 mN/m (see section 3.4), we

(47) Blinov, L. M.; Chigrinov, V. G. *Electrooptic Effects in Liquid Crystal Materials*; Springer-Verlag: New York, 1994.
(48) Kim, Y. B.; Olin, H.; Park, S. Y.; Chio, J. W.; Komitov, L.; Matuszczyk, M. *Appl. Phys. Lett.* **1995**, *17*, 2218.
(49) Cognard, J. *Mol. Liq. Cryst. Liq. Cryst., Suppl. 1* **1982**, *78*, 1.
(50) Papanek, J.; Martinot-Lagarde, Ph. *J. Phys. II Fr.* **1996**, *6*, 205.
(51) Barbero, G.; Durand, G. *J. Phys. II* **1991**, *1*, 651.
(52) Monkade, M.; Boix, M.; Durand, G. *Europhys. Lett.* **1988**, *8*, 697
(53) Collings, P. J.; Patel, J. S. *Handbook of Liquid Crystal Research*; Oxford University Press: Oxford 1997.

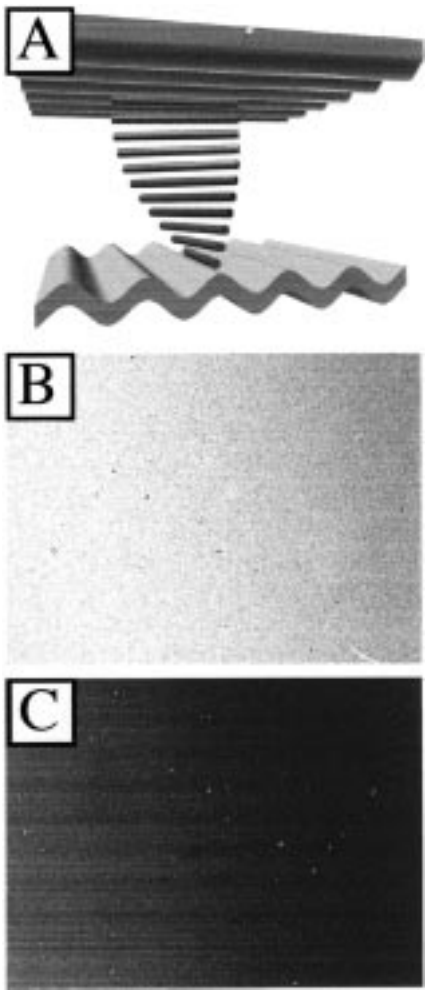

Figure 8. (A) Schematic illustration of a physically twisted (90°) nematic LC cell. The orientation of the LC near the surface is parallel to the sinusoidal grooves. (B) Polarized light micrograph (transmission mode) of a twisted nematic LC cell formed using obliquely deposited films of gold that support SAMs formed from propanethiol. The image was taken between cross polars. (C) Same as B but viewed between parallel polars. The thickness of the cell was 1 μm. The horizontal dimensions of the images in B and C are 1.1 mm.

calculate the strength of the azimuthal anchoring energy to be sufficiently large to permit the formation of twisted cells that are as thin as 0.5 μm. To test this prediction, we fabricated optical cells from SAMs formed from propanethiol on the surface of obliquely deposited films of gold. Analyses of AFM images of gold films supporting SAMs formed from propanethiol indicate the same level of anisotropy as seen with bare gold surfaces. Parts B and C of Figure 8 show the optical textures formed by polarized light transmitted though an optical cell filled with nematic 5CB, with a thickness of $\sim$1 μm. The bright image (Figure 8B) is caused by light transmitted through the cell and crossed polars: The dark image (Figure 8C) is caused by the extinction of light when the cell is placed between parallel polars. These optical characteristics indicate the presence of a twist deformation of 5CB within the cell, consistent with the prediction that the strength of azimuthal anchoring is sufficient to support twist within cells as thin as 0.5 μm. We were unable to construct cells of thickness less than 1 μm. The glass slides vary from flatness by $\sim$1 μm on lateral distances of a few centimeters, thus preventing the fabrication of cells having a spacing of less than 1 μm. In addition, when the cell thickness is less than 1 μm, the nature of elastic distortions within the LC is not well-understood.[29]

4. Discussion

A principal result of this study is identification of structural anisotropy within ultrathin obliquely deposited gold films that can provide an account of the preferred azimuthal orientations of LCs supported on these surfaces. Whereas visual inspection of AFM images does not reveal unambiguous anisotropy within these films, quantitative analyses of AFM images reveals an anisotropic roughness capable of orienting LCs with a strength of anchoring consistent with our experimental observations using twisted LC cells. Whereas quantitative analyses of images obtained by using, for example, electron microscopy are difficult to perform, we point out that a strength of scanning probe methods (AFM or STM) for characterization of rough surfaces is the ease with which quantitative analyses can be performed.

Although past studies[22−28] of obliquely deposited gold films have not used Ti as an adhesion layer between the glass substrate and gold, it is useful to compare our results obtained using AFM to the results of past studies using electron diffraction and return path ellipsometry. First, when using rates of deposition similar to those used by us, past studies[26] have reported contiguous films of gold to form for thicknesses of gold of $\sim$7 nm and greater. This observation is consistent with our measurements: we observed films of gold with thicknesses of $\sim$10 nm to be contiguous. Second, when characterizing films of gold with thicknesses of $\sim$10 nm, past studies[27,28] have not measured columnar growth nor the tilting of grains toward the direction of incidence of the gold. These observations are consistent with our results: we found no evidence of tilted grains nor columnar growth. Third, past studies[26−28] have observed tilted, columnar grains to form within thick gold films. Our preliminary measurements (not reported in this paper) of thick gold films by AFM also reveal a change in the structure of the gold films when the thicknesses exceed $\sim$30−50 nm.

A conclusion of our study is that the *elastic* energy stored within a LC supported on an obliquely deposited film of gold is sufficient to explain the formation of twisted LC cells when using these surfaces. While the elastic energy density has been considered in the context of the anchoring of LCs on rubbed polymer films and obliquely deposited SiO_x films, we point out that the elastic energy density in these systems is not the dominant contribution to the anchoring energy.[37,45,48] For example, the orientations of LCs on rubbed polymer films (e.g., polyimides) are largely due to the stress-induced alignment of the polymer chains in the near-surface region of the polymer film.[49] This point is illustrated dramatically when LCs are aligned on rubbed films of polystyrene: the direction of alignment of 5CB is perpendicular to the direction of rubbing (across corrugations in the surface).[29] For the case of obliquely deposited SiO_x films, it is important to realize that the level of roughness within these surfaces is substantially greater than obliquely deposited metals such as gold;[31]

thus, an evaluation of the elastic energy density using eq 9 for films of SiO_x is not valid. Rather, the orientations of LCs on SiO_x surfaces are dominated by changes in the orientational order parameter within the LC phase in the near surface region of the sample: a gradient in the order parameter of the LC can give rise to electrostatic contributions, for example, to the anchoring energy (so-called order-electric effects).[50−52] In short, our conclusion that the elastic mechanism of anchoring is important on obliquely deposited gold should not be taken to infer that such a description of anchoring is appropriate for other surfaces, nor does it rule out additional contributions to the anchoring energy of LCs on obliquely deposited films of gold. Indeed, our past reports of the orientations of LCs supported on obliquely deposited gold films covered by SAMs formed from odd and even alkanethiols demonstrate that mechanisms of anchoring other than elastic ones contribute to the behavior of LCs on these surfaces.[3]

The conclusion that structural anisotropy exists within obliquely deposited films of gold with an amplitude of ∼1−2 nm and a wavelength of ∼10 nm or less is significant for several reasons. First, it leads us to conclude that the binding of molecules (or aggregates of molecules) with dimensions comparable to those of the structural anisotropy can erase the anisotropy responsible for the uniform orientations of LC observed on obliquely deposited gold films. Adsorption-induced erasure of this structural anisotropy likely accounts for our past observations dealing the specific binding of proteins to ligands (e.g., antibody−antigen) hosted within SAMs on obliquely deposited films of gold. We reported that binding of proteins to ligands hosted on these surfaces erased the preferred orientation of LCs on these surfaces. After the protein was bound to the surface, the azimuthal orientation of the LC was found to be random. Second, the results reported in this paper suggest that specific adsorption of molecules that are small compared to the scale of the structural anisotropy may lead to changes in anchoring but that these changes in anchoring should preserve the symmetry of the obliquely deposited film of the gold. Indeed, our observations that odd and even alkanethiols lead to azimuthal orientations of LCs on these surfaces that are either parallel or perpendicular to the direction of deposition is consistent with that prediction. Third, the results in this paper suggest that it should be possible to prepare and characterize films of gold that systematically differ in their anisotropy (by variation of the manner of deposition of the gold). Methods that permit systematic control of anisotropy of the type found in obliquely deposited gold films will make possible, we believe, control of the threshold concentration of surface-bound analytes necessary to change the orientations of supported LC. These principles should, for example, permit amplification and transduction of lower concentrations of surface-bound proteins than were reported in our past studies.[7]

5. Conclusions

We report measurements of structure anisotropy within gold films obliquely deposited onto the surface of glass substrates. These gold films have an average thickness of 10 nm and are formed of grains with lateral dimensions of ∼20 nm and radii of curvatures of ∼50 nm. Although anisotropy within these films cannot be seen unambiguously by visual inspection of AFM images, a quantitative analysis of AFM images reveals that contour lengths, curvatures, and Fourier spectra of cross sectional profiles on nanometer scales (∼1−10 nm) do differ when measured parallel to the direction of the deposition of the gold and perpendicular to it. By using the Fourier spectra of cross sectional profiles, we calculate the elastic contribution to the azimuthal anchoring energy of a LC supported on these surfaces to be 0.015 mJ/m^2 and demonstrate that the magnitude of this contribution to the anchoring energy is sufficient to account for experimentally observed orientations of LCs supported on obliquely deposited films of gold. These results suggest a route to the design of obliquely deposited gold surfaces that differ systematically in their anisotropy; these surfaces will, we believe, be useful in future studies of analyte-induced changes in the orientations of LCs (e.g., for amplifying and transducing the binding of antibodies to surface-bound antigens).

Acknowledgment. This research was supported by the Office of Naval Research (Presidential Early Career Award for Scientists and Engineers to NLA) and by the National Science Foundation (CTS-9502263 and DMR-9400354).

CM9804822